Development and Applications of Cell Sorters Based on Hydrodynamic Filtration

Jinxuan Ding [1,†], Yuan Xie [2,†], Yixuan Zhang [3,†], Yuchi Zhang [4,*,†]

[1] The Cambridge Matignon School, Cambridge, USA

[2] Wuhan Britain-China School, Wuhan, China

[3] No.55 Middle School, Tianjin, China

[4] United World College, Changshu, China

* Corresponding Author Email: 15010140209@xs.hnit.edu.cn

† These authors contributed equally.

Abstract. Cell sorters is one of the key topics of physical research today. Cell sorters can sort cells, and through this process, specific cell types can be distinguished from other cell types contained in the sample based on the physical or biological properties of the sample. The homogeneous cell population obtained after sorting can be used for a variety of applications, including research, diagnostics and therapeutics. Researchers have made significant progress in cell sorters including the design principles optimization design techniques etc. Cell sorters based on hydrodynamic filtration possesses a channel and a sidewall which could be applied in particle transmission. In this paper, the research method, results, main findings in related research about the cell sorters based on hydrodynamic filtration are discussed. Suggestions for the development and application of the sorter based on hydrodynamic filtration are put forward. Overall, this paper could be a useful reference for those who would like to know sorters based on hydrodynamic filtration.

Keywords: Microchannel, liquid particles, particles position.

1. Introduction

A microfluidic cell sorter using cutting-edge approach for continuous concentration and sorting of micro particles through hydrodynamic filtration is introduced in the paper. The hydrodynamic device possesses a channel and a sidewall which could be applied in particle transmission.

High-quality sperm cells may be precisely manipulated and controlled using microfluidics and a variety of stimuli, such as chemical, mechanical, and temperature gradients. Furthermore, sperm and oocyte in vitro fertilization or sperm sorting using passive and active approaches can be guided by microfluidic systems. This gadget was first released in [1, 2] emphasizes successful technologies progressing toward clinical use or approaching commercialization in the male infertility sector with regard to microfluidic sperm sorting, manipulation, and analysis. We also assess a microfluidic-based device that makes it easier to non-invasively identify and sort living sperm for in vitro fertilization. Last but not least, [2] explores the commercial challenges brought on by microfluidic sperm sorting devices and suggests solutions and potential future directions. A design of experiments (DOE) methodology and COMSOL Multiphysics simulation modeling software were utilized by [3] to develop a microfluidic sperm sorting device (SSD) that could be produced rapidly, cheaply, and efficiently. Performance of SSDs is impacted by eight different factors. [4] proposed a simple microfluidic device that can hydrodynamically filter submicron particles (critical size 0.1 um) from a complicated sample without the need of a filter (minimum channel size 5 microns). The model takes into consideration hydrodynamic drag and real velocity profiles. [5] There is discussion of hydrodynamic filters' potential in wastewater treatment. The current state of the art in the field of hydrodynamic filtration is presented, and it is demonstrated that the known design options for hydrodynamic filters are classified into two characteristics: the presence or absence of a sludge liquid and the method of generating sludge with an additional force field. This is based on an overview of the preparation and regeneration of hydraulic oil systems. [6] made the argument that blood and blood

cells are significant indicators of numerous diseases. A quick and precise clinical diagnosis can be made by changing the physicochemical characteristics of blood cells using microfluidic tools. The history of microprocessing technology is reviewed in this essay, along with some design considerations for microfluidic devices and an overview of the technology in general, with a focus on biomedical applications.

This paper aims to provide a summarization of the recent advances of cell sorters based on inertial forces. In this paper, the research method, results, main findings, and future applications of each device and system will be introduced and explained in detail. In addition, possible suggestions and shortcomings of the device will be pointed out at the ending of each paper review.

2. Main body

2.1. Flowing particles in the focus channel by hydrodynamic filtration

Aoki et al. [7] used three methods to control flow or generate complex forces so that it can be incorporated into a fully integrated microsystem. In the micro channel shown in Figure 1, when the flow is slow enough and the particle is big enough, the liquid will not go to the channel on the other side. The liquid will stay the way to keep going through the main channel. Liquid will pass the side channel but a small amount of liquid will go though. The side channel cannot decide the size of the particle as well as how small the liquid particle can pass.

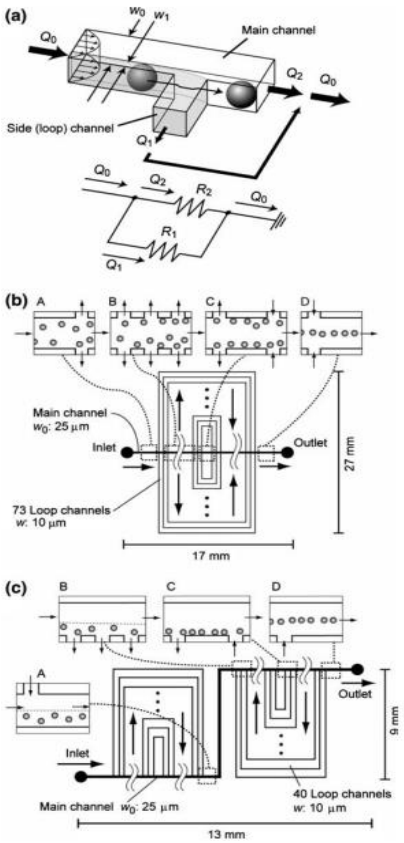

Figure 1. Schematic showing the behaviour of the particles at the branch points of the main channel and the corresponding resistive circuits using the main and ring channels

In a word, we can control the particles size the flow not in to the side of channel, since the micro channel structure which is designed based by the micro channel network. The particle focusing on the micro channel have many side channels on the both sides that will make the particle been split from the main channel and re-injections when the flow is flowing as shown in Figure 1 (b). The other method shown in Figure 1 (c) illustrates the split and re-injections of the particle. This microchannel has two sets of annular channels so that the fluid near the two sides of the wall can be gradually

separated. Compared to the first solution, this flow will allow more precise and efficient focusing of the particles.

It is then possible to freely control the size of the particles flowing into the side channels to complete the classification. By designing a network of microfluidic channels based on resistive and circuit simulations, and by precisely fabricating the structures in the microfluidic channels, we can freely control and efficiently control the size of the particles flowing into the side channels.

In a micro fluidic control device, main channel and two sides of channel should be symmetrical. The width and size of the channel must be layered according to the size of the example to get the desired effect. With those requirements, the device is fabricated. Microdevice 1 is used at the beginning to try to check how those referenced particles pass through the confluence point after being concentrated in the center main channel. Figure 2 (a) shows a photograph of the flow around the fluorescent particles as they pass through the exit of main channel to argue our idea, when the inlet flow rate is 2.0mL/min. Due to the high speed (*100 mm/s), the trajectory of the fluorescent particles takes on a linear appearance.

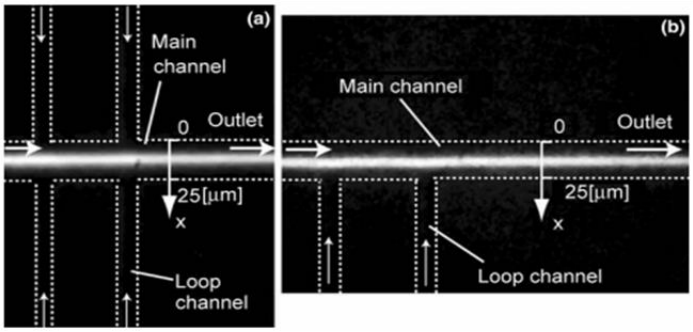

Figure 2. Particles flowing near the outlet of (a) 1 and (2) b

The operation is simple but the first scheme is not efficient in focusing particles. In fluid flow is separated and recombined through both main channel and the loop channels on both sides, so the two peaks often appear as shown in the Figure 3 (a), (b), (d) is even smaller than 3 (a), (b). In order to better concentrate the particles in the center, it is attempted to increase the total flow through in to the loop channel by changing the design of the microchannel. To achieve this/fulfill this goal, the efficiency of a circulation channel with a sharply increasing number of microchannels should be used, because the proportion of the diversion rate at each branch of point is not change.

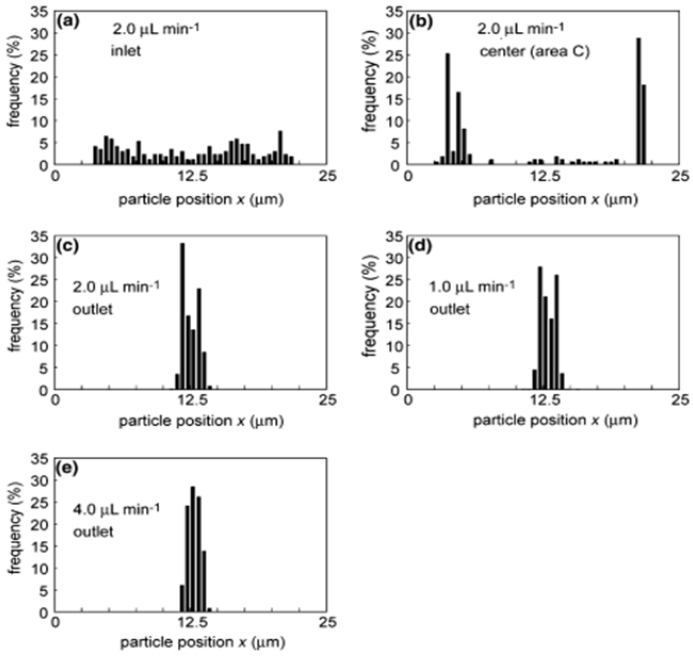

Figure 3. Histograms shows that distributions in Microdevice 1

Histograms of the position of the liquid particles in zone A in Figure 1 (c) (inlet flow rate of 2.0l/min) and the histogram of the particles near the outlet position at the inlet when the flow rate is 1.0, 2.0 or 4.0l/min. The actual histograms of the positions of these particles at inlet flow rates of 1.0, 2.0 or 4.0l/min are shown in Figure 4. Overall, the sorting efficiency of this device is not affected by the flow rate, which facilitates the use of the proposed system as an important part of an integrated flow system.

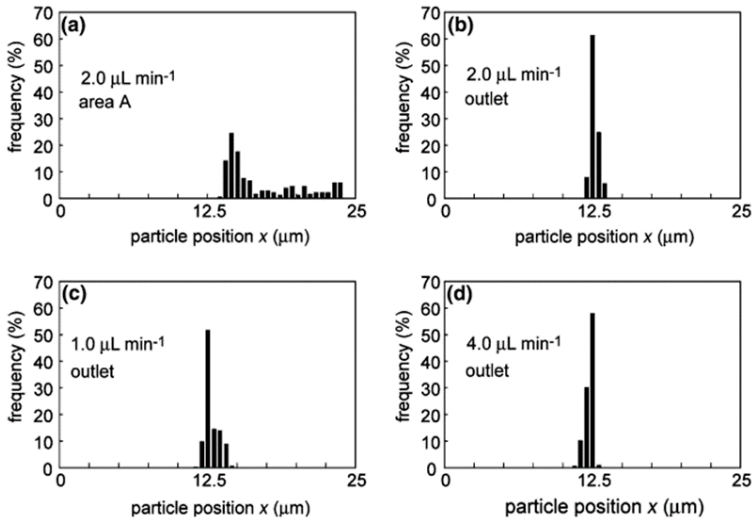

Figure 4. Illustrates a histogram of the distribution of particle positions in microdevice 2

2.2. Cross-flow filters with hydrodynamic focusing to improve microfluidic particle separation

Cross-flow filtration augmented by hydrodynamic focussing was suggested by Chiu et al. [2] as the method for particle separation on a microfluidic chip. Particles in the sample flow are pushed to one side of the microchannel by using the side buffer flow, aligning them to pass through the filter. The filter also gets a bigger pressure gradient at the same time to increase separation effectiveness.

The proportion of the sample flow that is filtered is first calculated by simulating the flow field within the microfluidic device using flow and pressure field simulation. In the absence of buffered flow, the bulk of the sample flow enters the main channel and diffuses across the filter array. Filtered dust and some of the water flow will make their way into the trash channel. When the buffered flow is injected from the side channels, the majority of the flow is driven into the filter, forcing the majority of the particles through the filter. When the buffer flow and the sample flow are equal, 62% of the sample flow is filtered into the waste channel. When the buffer stream flow rate is raised to 40 l/min, the whole sample stream is filtered into the waste channel. When there is no buffer stream, just a tiny portion of the sample stream is filtered by the filter. The sample stream diffuses over the microchannel as an alternative. When a buffer flow is provided, the sample flow is likewise gradually compressed as it moves in the direction of the filter and all the way into the waste stream channel. As the buffer flow to sample flow ratio rises, the sample flow's width falls.

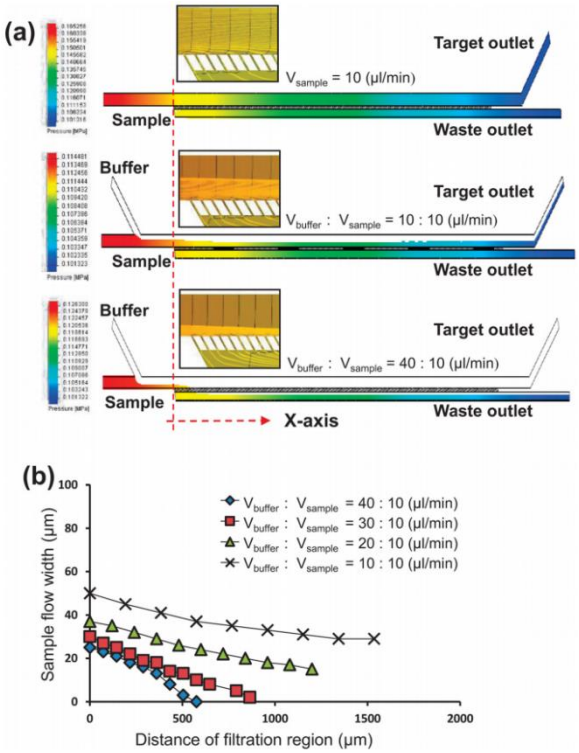

Figure 5. (a) Sample flow trajectory plots generated by our three-dimensional flow simulation model. The color denotes the gradient's certainty. The close-up views used in the insets to locally depict the sample flow paths around the filtration zones. (b) The correlation between the sample flow's width and the separation from the filter region's start

Additionally, the method of fabrication uses cross-flow filtering and soft photolithography to create microchannel devices. On the defining pattern of a (100) p type 4 in. wafer, positive photoresist was spun coated. For the purpose of obtaining a silicon die, deep reactive ion etching (DRIE) (SAMCO RIE-800 iPB, SAMCO, Inc., Fushimiku, Kyoto, Japan) was used to etch the silicon and produce features. Trifluoro-1, 1, 2, 2-tetrahydrooctyl trichlorosilane was used to silicify the silicon moulds before polydimethylsiloxane, or PDMS, was mixed with it and applied to the silicon mounds (Sylgard 184, Dow Corning, Midland, MI, USA). The PDMS mixture was cured, peeled, and sliced after degassing. The inlet and outflow of the microchannels were then defined by punching the PDMS.

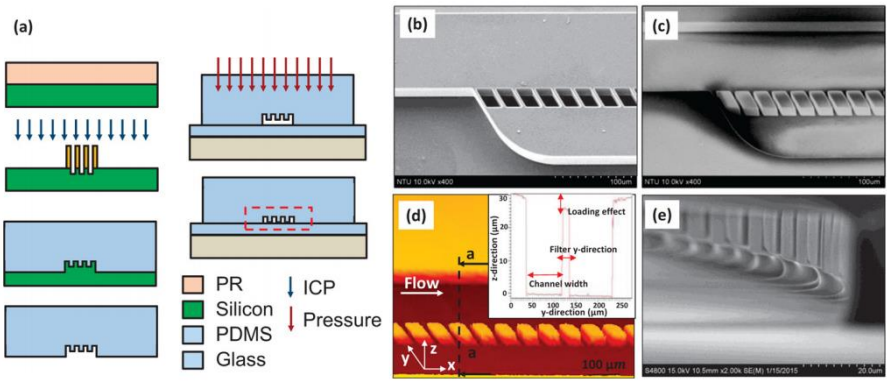

Figure 6. (a) The way our devices are made. (b) The silicon mold had a longer depth in the filter gap and a shallower opening area (c) An SEM image of a microchannel with microfilters near the intake. The filters were spaced apart by four spaces. (d) An optic type surface analyzer was used to measure the PDMS microchannel height. (e) The majority of the filter regions were glued to the substrate using the pressured PDMS bonding technique at a pressure of 15kPa

The separation mechanism was then developed using numerical simulation and finite element analysis. Simulations with various flow combinations of sampled and buffered flows were done to

verify the flow focusing effect. Phosphate buffered saline (PBS) with a density of 1 10kg/m and a dynamic viscosity of 1.05mPa s was actually used to approximate the buffer stream. The sample stream contained suspended particles. The sample stream, which is a combination of solid particles and liquid, has a relative viscosity (u,) that may be explained by the viscosity relative to the liquid phase (PBS). The relative viscosity is influenced by the volume proportion of solid particles as well as their size and concentration.

The separation mechanism was then developed using numerical simulation and finite element analysis. Simulations with various flow combinations of sampled and buffered flows were done to verify the flow focusing effect. Phosphate buffered saline (PBS) with a density of 1 10kg/m and a dynamic viscosity of 1.05mPa s was actually used to approximate the buffer stream. The sample stream contained suspended particles. The sample stream, which is a combination of solid particles and liquid, has a relative viscosity (u,) that may be explained by the viscosity relative to the liquid phase (PBS). The relative viscosity is influenced by the volume proportion of solid particles as well as their size and concentration.

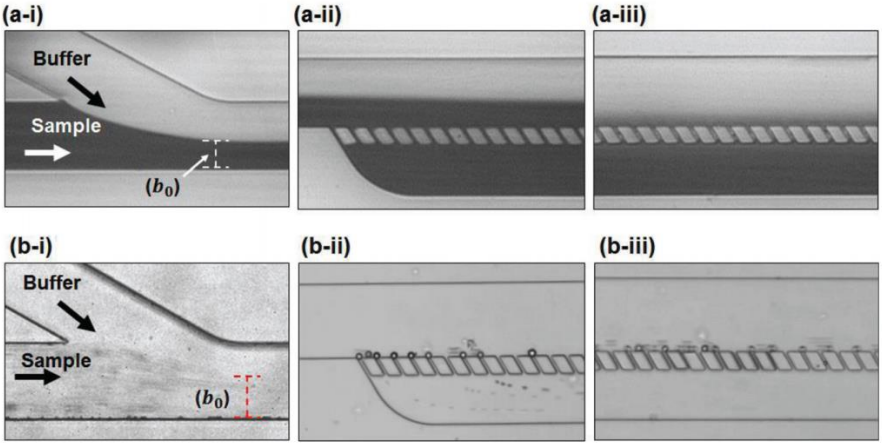

Figure 7. (a) The sample flow (such as DI water) and buffer flow created a virtual flow boundary (e.g., blue ink). (a-i) When two flows first mixed, the sample flow (b0) had a width of 50lm. (A–II) As the flow moved through the microchannel, the sample flow width gradually shrank. The majority of the sample flow was forced through the filter and out the waste exit (figures a–iii). (b) The photographs of the particles going through the microchannel revealed the three steps of the filtration process

The microscopic images of the particle-containing solution prior to filtering and the images of the particles retrieved from the target and waste outputs are shown in Figures 8 (a) through (c). Filtration of V_{buffer}: V_{sample} at a 40:10 (µl/min) flow rate. Figure 5 (A) shows that a mixture of two different particle sizes was present, and Figures 5 (b) and 5 (c) show that high purity particles of the sizes 10.6um and 2.7um were primarily present at the target outlet and waste outlet, respectively. Further measurements from flow cytometry data are shown in Figures 5 (d)–5 (f) (plotted as forward scattering FSC and side scattering SSC). The data were separated into three distinct populations of particles with diameters of 2.7mm, 10.6mm, and 15mm. For particle counting, 15m reference particles (ACBP-150-10, Spherotech, Inc., Lake Forest, IL, USA) were employed at established concentrations. The group count as a proportion of all particle occurrences is shown by the counts close to the gating group. For particles with a diameter of 2.7m and 10.6m, the sample inlet concentration was 42% and 43%, respectively. The total number of 2.7um and 10.6um particles was calculated using a concentration of 3.3% of 15um particles.

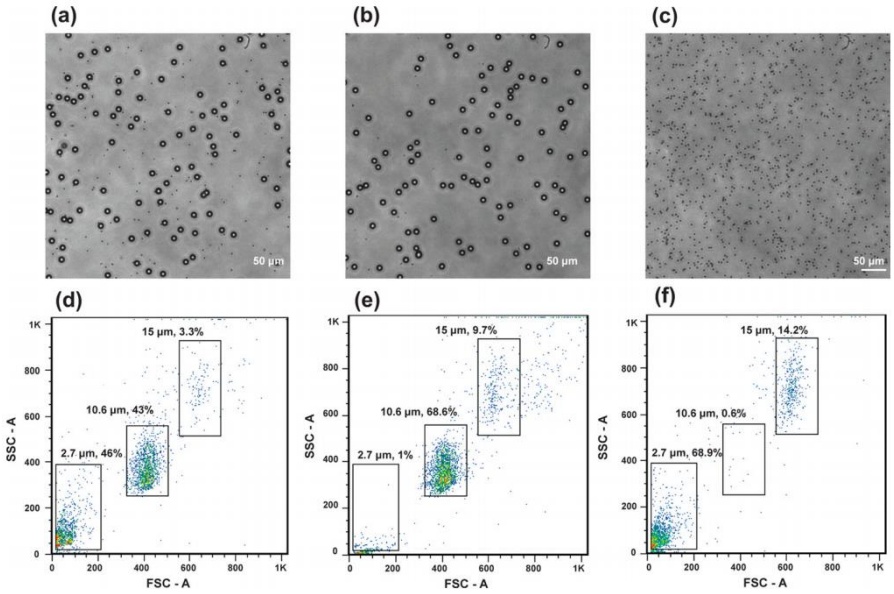

Figure 8. Representative microscopic images of (a) the mixture of the microparticles of 2.7m and 10.6m before separation, (b) the samples collected from the target outlet after separation, and (c) the samples taken from the waste outlet after separation are shown (c)

To improve the separation efficiency overall, a unique staggered flow filtration technology is suggested. A high-pressure polydimethylsiloxane bonding technology is created to construct devices with a high spreading ratio filter structure in order to combat the micro-loading effect. For larger flow rates, the filter structure offers a more durable construction. It was possible to attain sample flow rates of up to 50pl/min and buffer flow rates of up to 200μl/min. The results of the tests indicate that the suggested mechanism has a lot of potential as a low-cost, process-accumulative technology that may support particle and cell separation applications. It also has high recovery and high purity.

2.3. Filtration, concentration and classification for hydrodynamic particles with microfluidics

M. Yamada *et al.*, developed a new series of devices in order to separate microfluidic particles [9]. This series of novel devices propose a new method of filtering microfluidic particles. These devices all wisely exploit the flow profile to filter particles based on their size. Three variants that belong in this series of devices are shown as examples and initial models. They differ in the parameters of their microfluidic tunnels. They are meant to be used under certain different circumstances. To be specific, each one of them is best suited for either a limited range of sizes of the particles or a particular type of particles. These constraints are set up so that best sorting effects can be reached.

It can be discovered without difficulty that even though they differ in the size of the microfluidic channels (the length and diameter of the channels), their basic structures are the same, which means that they work under the same principle.

Figure 9 shows the commonality of this type of devices: they all rely on a main channel and several side channels. The side channels, when equipped with an appropriate diameter, can draw microfluidic particles of a particular size out from the original stream in the main channel, thus satisfying the purpose of filtering particles in accordance with their size. No matter what the size of the side channels are, they can always decrease the fluid inside the main channel if the pressure inside the main channel is large enough to exceed a specific value, which is always true in order to keep the fluid moving, therefore achieving the purpose of concentration in the microfluidic level. The value mentioned above is determined collectively by several different factors, among them the diameter of the side channels. Thus, by manipulating the diameter of all side channels, both con centration and filtration can be controlled.

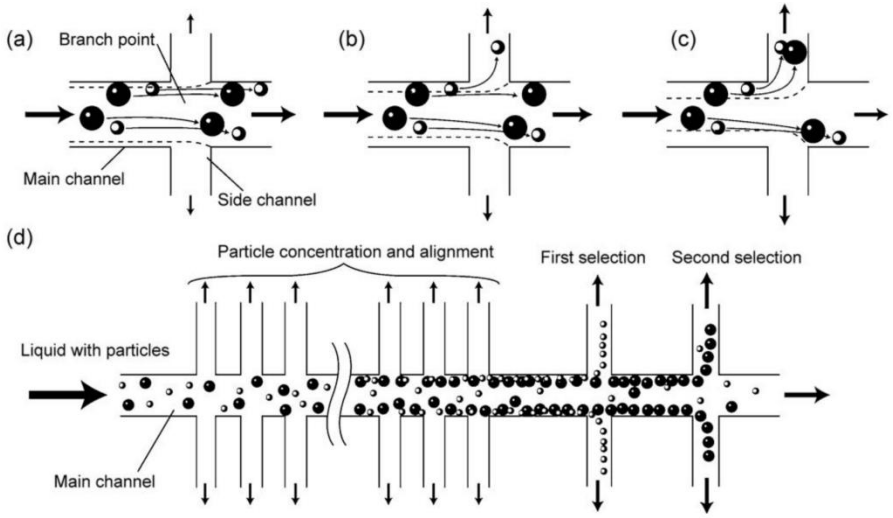

Figure 9. The working mechanism of the device. The flow rates are (a) low, (b) medium, and (c) high. The virtual boundaries of the flows are shown by broken lines. (d) Particle classification and concentration in a microfluidic device similar to the ones proposed

Experiments and schematic for Type I (the first model) are shown in Figure 10. This type of device is intended to sort particles that are relatively large, with a diameter of more than~2μm. In this specific experiment, microfluidic particles with a diameter of 2.1μm are used as "small" particles, while those with a diameter of 3.0μm are used as "large" particles. To see easier, the two different particles selected have different colors.

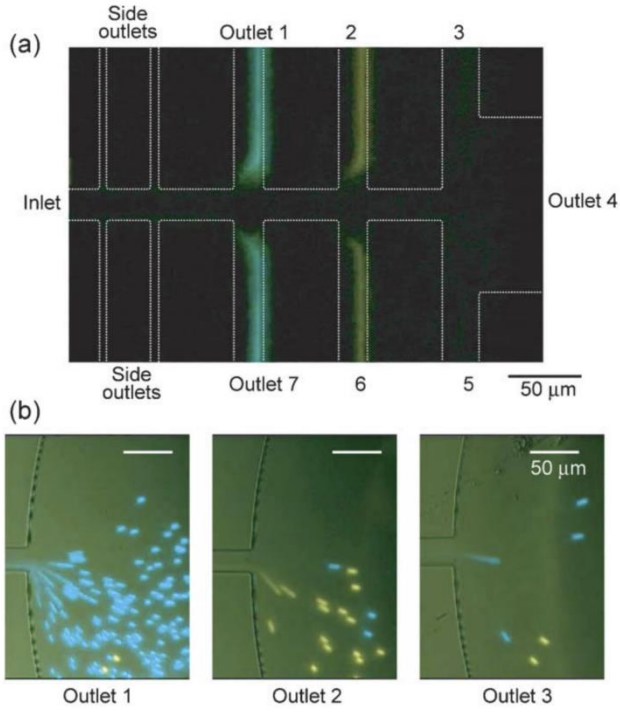

Figure 10. Particles in the Type 1 microdevice. (a) Concentrated and separated particles at each outlet. (b) Particles flowing into each outlet.

Experiments and schematic for Type II are presented in Fig. 11. This type of device is intended to sort particles that are relatively small, though the researchers did not give a specific numeral for the diameter of the particles. In this specific experiment mentioned in the paper, microfluidic particles with a diameter of 1.0μm are used as "small" particles, while those with a diameter of 2.1μm are used as "large" particles.

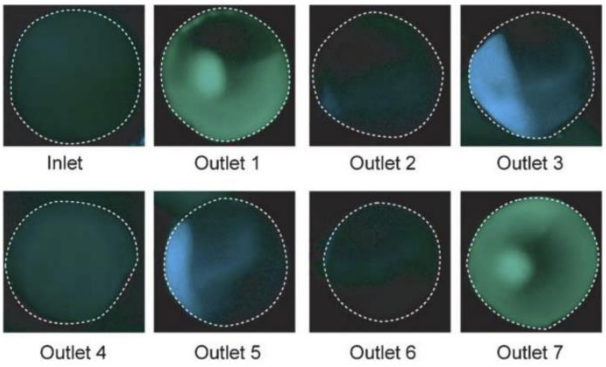

Figure 11. Particle concentration and classification in the Type 2 microdevice. Photographs show the inlet and classified particles in outlets

Experiments and schematic for Type III are illustrated in: This type of device is intended to sort living cells. To be specific, leukocytes are used. In this experiment, the device enriched (purified and concentrated) the leukocytes, as can be seen in Figure 12.

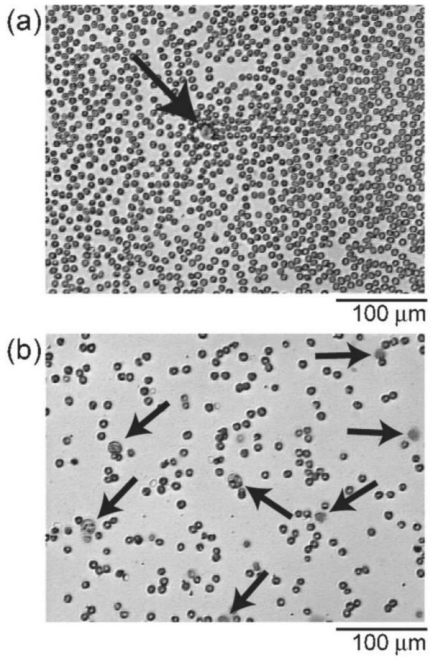

Figure 12. Leukocyte enrichment. (a) Blood cells before filtration, and (b) blood cells after filtration, stained on a glass slide. Leukocytes are identified with arrows.

Overall, it is found that the three models presented in the passage mainly differs in their differences in the dimensions of the channels. With such changes in the future, this series of devices can suit much more conditions soon. However, the construction of such an equipment may require certain time, effort and accuracy. Integration of such devices with other equipment or other types of the same series of the device can be experimented.

2.4. Hydrodynamic filtration for particle sorting: Channel aspect ratio effects on microfluidic-chip design

Chun et al. [10] evaluated the flow rate and pressure drop in microfluidic networks with several branches through the development of a 3D analytical model. It is demonstrated how a hydrodynamic filtration chip with a rational design can sort particles.

First, the following is a summary of the design processes for the model framework of hydrodynamic filtration (HDF).

Assuming that convection occurs more quickly than diffusion and that mixing of the two streams is gradual, and that the inertial lift force of the suspended particle from the channel wall is

insignificant. The following equation describes the velocity field caused by the pressure gradient after the flow fraction in the rectangular microchannel has been computed step by step:

$$\mu\Delta^2 u = \nabla P. \tag{1}$$

Where μ is the fluid viscosity.

Then the 3D velocity profile of fully- developed flow through a rectangular channel is expressed as:

$$u_z\,(x,y) = \frac{4H^2}{\pi^3\mu}\frac{\Delta P}{L}\sum_{n=odd}^{\infty}\frac{1}{n^3}\left[1-\frac{\cosh\left(\frac{n\pi x}{H}\right)}{\cosh\left(\frac{n\pi W}{2H}\right)}\right]\sin\left(\frac{n\pi y}{H}\right). \tag{2}$$

Where W, H, L denote the width, height, and length, respectively. The channel length is subjected to the pressure decrease.

The following equation can be used to calculate the volumetric flow rate Q via a channel's cross-sectional area:

$$\iint_{-\frac{W}{2}\leqslant x\leqslant\frac{W}{2},\ 0\leqslant y\leqslant H} Q = \left(\frac{WH^3}{12\mu}\frac{\Delta P}{L}\right) f(H,W). \tag{3}$$

The flow function f is thus given by and ΔP/Q represents the hydraulic resistance:

$$f = 1-\frac{192}{\pi^5}\frac{H}{W}\sum_{n=odd}^{\infty}\frac{1}{n^5}\tanh\left(\frac{n\pi W}{2H}\right). \tag{4}$$

The fractional flow function can be derived similarly as the equation (3),

$$\iint_{-\left(\frac{W}{2}-WC\right)\leqslant x\leqslant\frac{W}{2}-WC,\ 0\leqslant y\leqslant H} f_f = \frac{2X}{W}-\frac{192}{\pi^5}\frac{H}{W}\sum_{n=odd}^{\infty}\frac{1}{n^5}\frac{\sinh\left(n\pi X/H\right)}{\cosh\left(n\pi W/2H\right)}. \tag{5}$$

Then in the following subsection, microfluidic-chip with channel networks was presented through Figures 13 and 14 and relevant calculations.

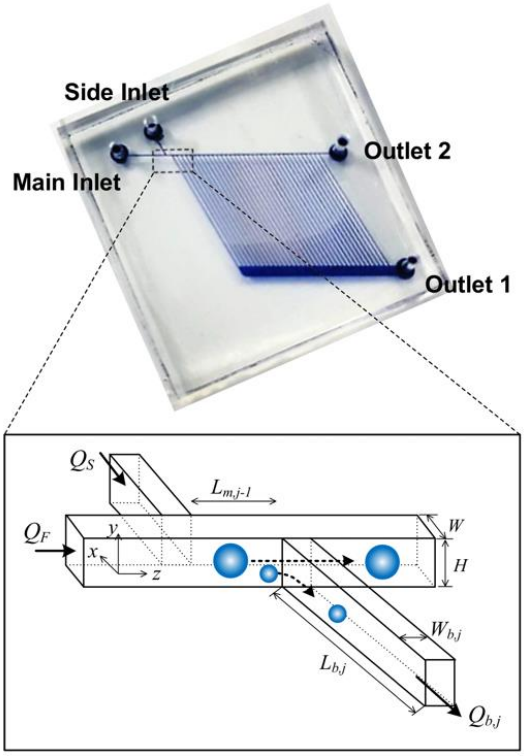

Figure 13. The schematic of the flow fraction in a microchannel with a branch angled at a 60° angle to the main channel is shown on the model HDF microfluidic-chip created for biomodal sorting. In light of the streamlined sorting, bimodal particle separation is taken into consideration, where particles of small size flow into the branch channel and large size travel along the main channel

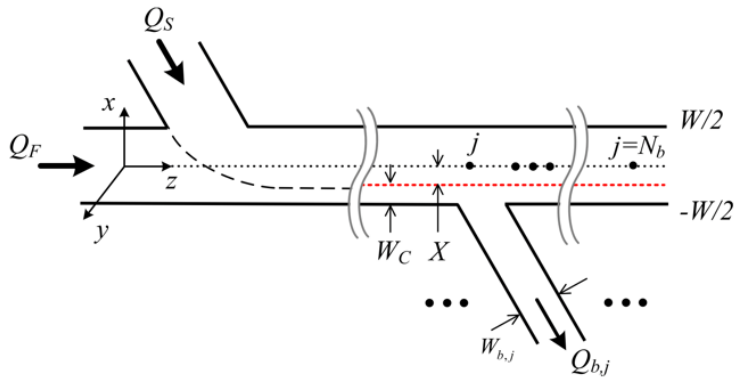

Figure 14. Nb represents the total number of branch channels, and j is the index of the branch point in the channel network design's schematic top view using the proper coordinates

By the given Equation (3), it is possible to express the flow stream that was redirected into the first branch channel as:

$$\iint_{-W/2 \leqslant x \leqslant -(W/2-W_c)} Q_{b,1} = \left(\frac{WH^3}{12\mu}\frac{\Delta P}{L}\right) f_b. \tag{6}$$

Also by the Equation (4) and (5), the flow function is obtained:

$$f_b = \left(\frac{W-2X}{2W}\right) - \frac{192}{\pi^5}\frac{H}{W}\sum_{n=odd}^{\infty}\frac{1}{n^5}\frac{\sinh\left(\frac{n\pi(W-2X)}{4H}\right)\cosh\left(\frac{n\pi(W+2X)}{4H}\right)}{\cosh\left(\frac{n\pi W}{2H}\right)}. \tag{7}$$

The volumetric flow rate in the first branch equals $Q_{b,1}=\xi Q_{m,0}$ based on Equations (6) and (7), and the residual flow is $Q_{m,1}=(1-\xi)Q_{m,0}$, where the ratio of flow fraction can be understood as the ratio of the flow rate between the branch stream and main stream. It is interesting that these relations can be used across the entire channel network.

Since all channels are exposed to the air and the yielding from each outlet is the same, pressure drops are described using Equation (8):

$$\sum_{j=0}^{k-1}\Delta P_{m,j} + \Delta P_{b,k} = \sum_{j=0}^{N_b}\Delta P_{m,j} = \Delta P \quad for \quad k = 1 \sim N_b. \tag{8}$$

The pressure drops at each branch are calculated by processing those partial volumetric flow rates for the focused stream, and each length of a specific branch channel was ultimately represented utilizing the relationship between the partial volumetric flow rate and flow function:

$$L_{b,j} = \frac{W_b H^3}{12\mu}\frac{\Delta P_{b,j}}{Q_{b,j}}\left[1 - \frac{192}{\pi^5}\frac{H}{W_b}\sum_{n=odd}^{\infty}\frac{1}{n^5}\tanh\left(\frac{n\pi W_b}{2H}\right)\right]. \tag{9}$$

Table 1 provides a summary of the parameters used for each group in the computations and model validation. Matlab (Mathworks, MA) was used to solve the model's framework, and the design properties it produced were compared to those from flow simulations to ensure their validity. COMSOL Multiphysics (Version 5.2a) was used to simulate the 3D flow in the rectangular channel using the finite element technique.

Table 1. The width of each branch, W_b, is set to 40μm, and the length of the first branch, $L_{b,1}$, denotes the longest branch, among other design parameters and related values

Input				Estimated		
H/W	$H(\mu m)$	$W(\mu m)$	H/W_b	N_b	$L_{b,1}(\mu m)$	ξ
0.5	68	135	1.7	17	7437	0.046
1.0	90	90	2.3	18	4981	0.081
2.0	135	68	3.4	13	3301	0.127
2.5	158	63	4.0	11	2980	0.145

The equation of motion is integrated using the velocity-Verlet approach while still taking into account the particle tracking simulation.

The Stokes Law specifies the viscous force exerted on a spherical particle:

$$F_{drag} = -6\pi\mu a_p\left[u_p(r,t) - u(r)\right]. \tag{10}$$

Where is the drag coefficient.

Following a collision, the particle's velocity is then given as

$$u_p^* = u_p - 2\left(n \cdot u_p\right)n. \tag{11}$$

An inverted microscope (Eclipse Ti-E, Nikon, Japan), a 5M pixel sCMOS digital camera (Zyla, Monochrome Cooling, ANDOR, UK), and NIS Elements software can all be used to detect streaks caused by particle transport. In this study, fluorescent polystyrene emulsion (Thermo Fisher Scientific Inc., MA) was dispersed in 0.2 percent (w/v) Triton X-100 to create bidis perse suspensions of spherical particles. Movies were programmed to play at half their normal pace. All of the figures in Figure 15 are displayed at the same scale. The channel network architecture based on our concept is shown in Figures 15 and 16 at various aspect ratios. The complete results summary is shown in Table 1.

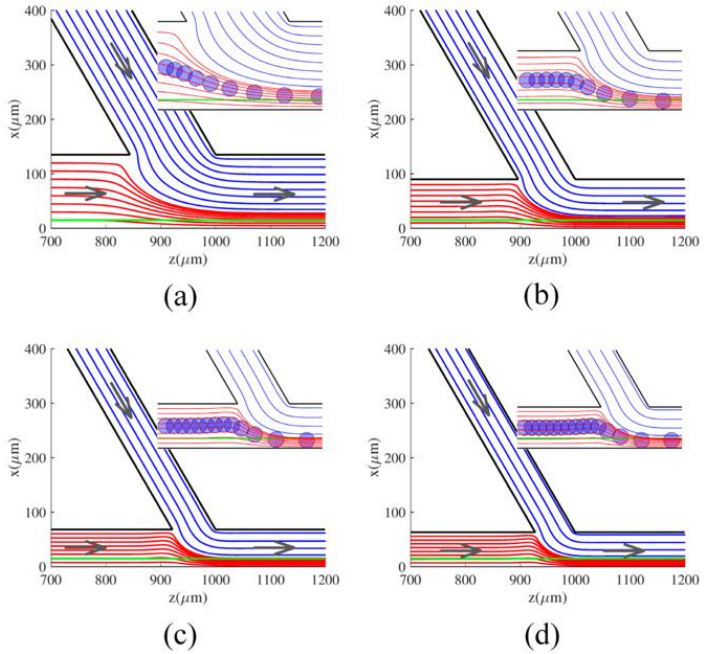

Figure 15. The following channel aspect ratios were used to calculate the streams and particle trajectory: (a) H/W=0.5; (b) H/W=1.0; (c) H/W=2.0; and (d) H/W=2.5. Here, the lines denoting the side flow, main flow, and W_c (=15μm) are colored blue, red, and green, with arrows pointing in the direction of each flow. Every 0.8 milliseconds, the trajectory of a particle with a initial position at x=W/2 and a radius of 12m was recorded

As the aspect ratio H/W rises or as the branch point j approaches closer to the end of the main channel, the pressure decreases and the average velocity decreases accordingly, as seen in Figure 16. There are observed quantitative agreements between the analytical results and the numerical simulations. To remove the minimally bothersome pressure drop caused by the apertures at the entry of each branch channel, the pressure drop across the main channel's cross-section is averaged in the simulations.

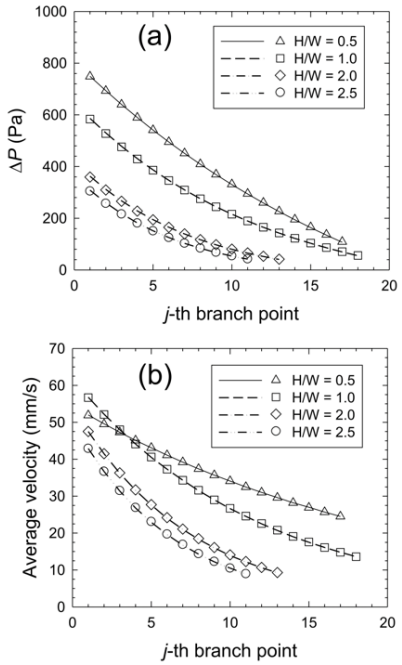

Figure 16. The accompanying open symbols on each line represent the numerical outcomes of our model's analysis, which are reflected in each line. Changes in (a) pressure drop and (b) average velocity at each branch point with changes in aspect rates

The comparison of the flow fraction and the truncation width W_c at each branch point between the model framework and numerical simulations is shown in Figure 17 as well. The volumetric flow rate, which can be estimated by numerically integrating the trapezoidal rule over the cross-section of the channel at each branch point, determines the ratio of the flow fraction.

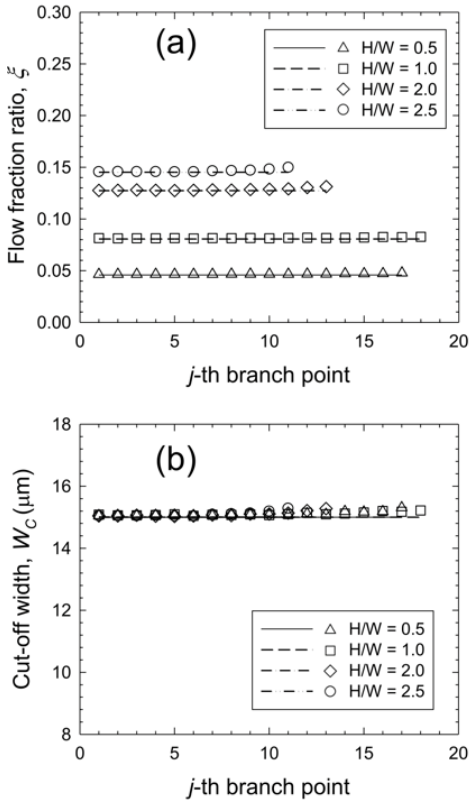

Figure 17. Results of comparisons between our model framework (each line) and computational simulations (open symbols) for (a) the ratio of flow fraction ξ and (b) the cut-off width Wc at each branch point with different aspect rates

Figure 18 shows the flow lines and particle trajectories to illustrate the flow fraction at branch sites, using the first branch region as an example.

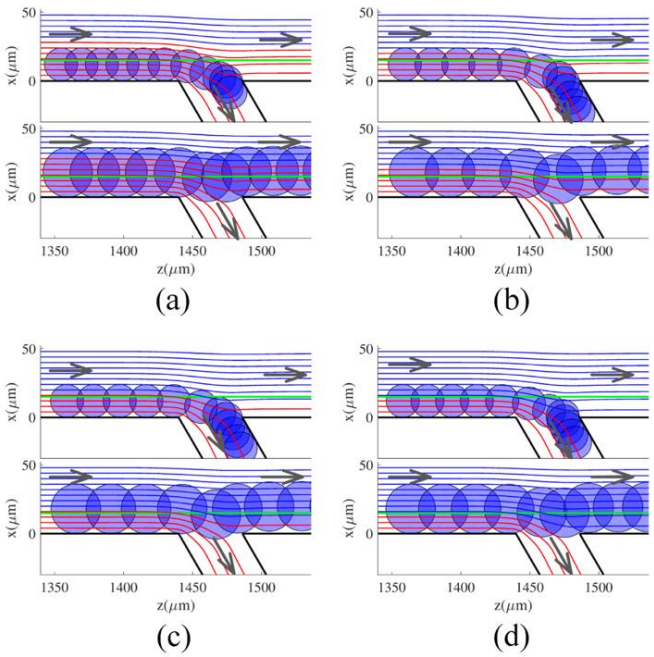

Figure 18. Aspect ratios of (a), (b), (c), (d), and (e) H/W=0.5, 1.0, 2.0, and 2.5 were used to determine the streams and particle track in the first branch region. Small (a_p=12μm<W_c) and large (a_p=18μm>W_c) particles are displayed individually for non-overlapped viewing. The settings were the same as in Figure 3 here, with each trajectory being taken every 0.6ms

Overall, the research results can be summarized as follows. Firstly, the analytical findings that the model produces are quantitatively consistent with the numerical results of the flow simulations and are tested against the particle tracking simulations. It should be stressed that smaller microfluidic chip sizes and pressure decreases result from the fewer and shorter branches found in rectangular microchannels with deep geometries (i.e., high aspect ratios). Secondly, the pressure drop, average velocity, and the flow fraction scale at each branch point for various channel aspect scales were all approximated as constitutive features of the flow field and the actual design. As the channel aspect scale rises (high aspect scale), the average flow velocity falls while the scale of flow velocities across the branch points rises. Thirdly, rather of using non-linear regression iterations to solve the current model framework, sequential approaches are used instead. This is helpful for predicting a number of unknown variables, which in this case should be the quantity of branch channels and each channel's length. In addition, our findings show that improving sorting efficiency and rational HDF chip design are both positively impacted by small modifications in channel aspect ratios.

However, the effect of pipe surface roughness was omitted. Furthermore, none of the uncertainties of these estimated values were taken into consideration and no error bars provided leads to a lack of stating physical meanings of the gradients, intercepts, etc.

As for the avenue of improvement, the effects of other external variables like the angle between branches and the main channel, surface roughness, etc. on this device could be conducted following and the iterations based on the nonlinear regression method can be put into use. Manufacture the prototype, do experiments, and collect and analyze the relation in average velocity, pressure drop, flow fraction ratio and aspect ratio to find out whether there are any ignored uncertainties or errors which were not presented through the simulation.

3. Conclusion

In this paper, the recent advances of sorters based on hydrodynamic filtration are summarized, among them both new devices and mathematical equations are presented. The main conclusions can be drawn as follows: (1) With the development of the technologies of fabrication, concepts that involve actions in the micro level will only become more and more popular; (2) For the field of fluidics, the shift to microscopic levels will only make it even more and more popular, because at such a level of sizes, physics of fluids can be connected with biology; (3) Many microfluidic devices are currently being invented, tested and fabricated. Among them, devices for filtering particles are occupying a considerable part.

Based on the current work, future research should be devoted to: (1) The development of more devices for microfluidic separation that can be occupied under different circumstances; (2) The connection between biology with physics, especially on the cellular level, or the microfluidic level.

References

[1] Khodamoradi, M., Rafizadeh Tafti, S., Mousavi Shaegh, S. A., Aflatoonian, B., Azimzadeh, M., & Khashayar, P. (2021). Recent microfluidic innovations for sperm sorting. Chemosensors, 9(6), 126.

[2] Phiphattanaphiphop, C., Leksakul, K., Phatthanakun, R., & Khamlor, T. (2020). A novel microfluidic chip-based sperm-sorting device constructed using design of Experiment Method. Scientific Reports, 10(1).

[3] Samuel, R., Feng, H., Jafek, A., Despain, D., Jenkins, T., & Gale, B. (2018). Microfluidic—based sperm sorting & analysis for treatment of male infertility. Translational Andrology and Urology, 7(S3), S336–S347.

[4] Fouet, M., Mader, M.-A., Iraïn, S., Yanha, Z., Naillon, A., Cargou, S., Gué, A.-M., & Joseph, P. (2016). Filter-less submicron hydrodynamic size sorting. Lab on a Chip, 16(4), 720–733.

[5] Devisilov, V., & Sharai, E. (2019). Hydrodynamic filters in hydraulic fluid cleaning system of Hydraulic Drive. IOP Conference Series: Materials Science and Engineering, 492, 012025.

[6] Catarino, S. O., Rodrigues, R. O., Pinho, D., Miranda, J. M., Minas, G., & Lima, R. (2019). Blood cells separation and sorting techniques of passive microfluidic devices: From fabrication to applications. Micromachines, 10(9), 593.

[7] Aoki, R., Yamada, M., Yasuda, M., & Seki, M. (2008). In-channel focusing of flowing microparticles utilizing hydrodynamic filtration. Microfluidics and Nanofluidics, 6(4), 571–576.

[8] Chiu, Y.-Y., Huang, C.-K., & Lu, Y.-W. (2016). Enhancement of microfluidic particle separation using cross-flow filters with hydrodynamic focusing. Biomicrofluidics, 10(1), 011906.

[9] Yamada, M., & Seki, M. (2005). Hydrodynamic filtration for on-chip particle concentration and classification utilizing microfluidics. Lab on a Chip, 5(11), 1233–1239.

[10] Chun, B., & Chun, M.-S. (2019). Effects of channel aspect ratio on microfluidic-chip design of hydrodynamic filtration for particle sorting. Journal of Physics D: Applied Physics, 52(22), 225301.